

Supplementary Information

Tuning high-order multiexciton properties of CdSe quantum dots via size and surface modification

Raktim Baruah,^{a,b,†} Krishan Kumar,^{a,b,‡} Jan Dellith^b and Maria Wächtler^{a,*,†}

^aChemistry Department and State Research Center OPTIMAS, RPTU Kaiserslautern-Landau, Erwin-Schrödinger-Str. 52, 67663 Kaiserslautern, Germany.

^bDepartment Functional Interfaces, Leibniz Institute of Photonic Technology Jena, Albert-Einstein-Straße 9, 07745 Jena, Germany.

[†] Current address: Institute of Physical Chemistry and Kiel Nano, Surface and Interface Science (KiNSIS), Kiel University, Max-Eyth-Straße 1, 24118, Kiel, Germany.

E-mail: waechtler@phc.uni-kiel.de

[‡] Institut für Physik, Carl von Ossietzky Universität Oldenburg, 26129 Oldenburg, Germany.

TEM

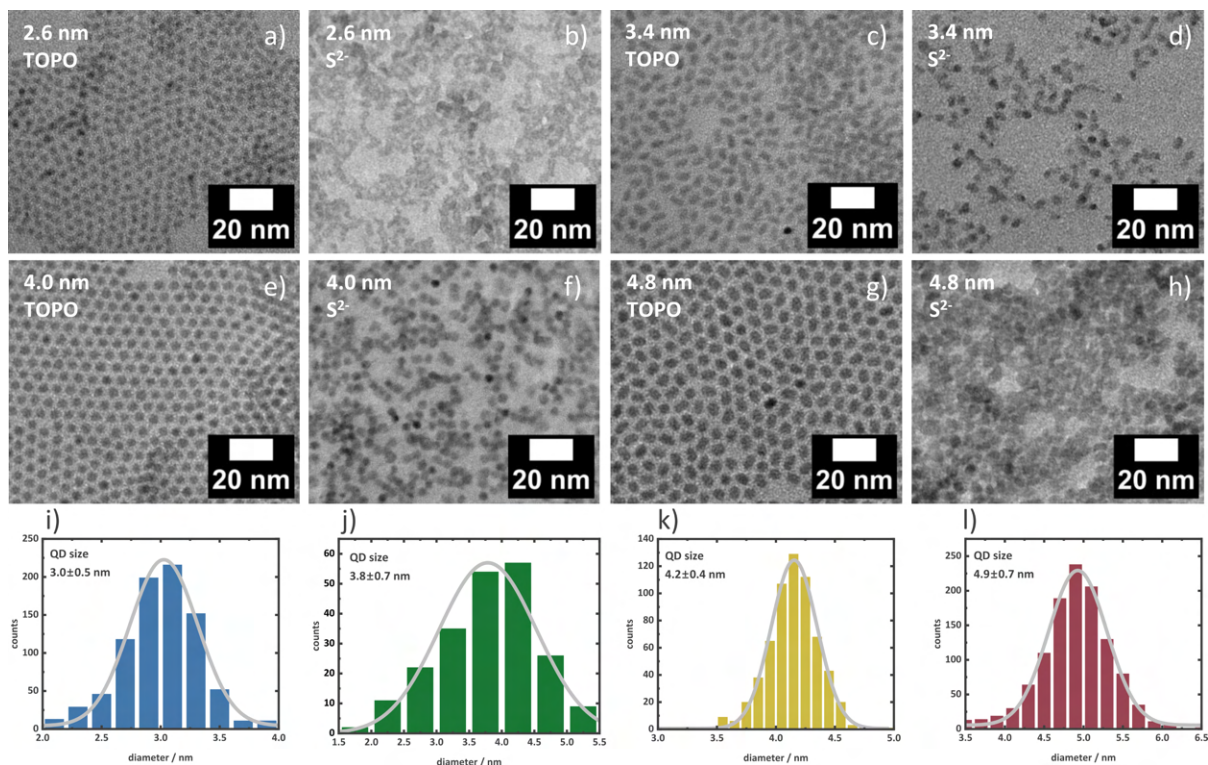


Fig. S1 TEM images collected for the TOPO- and S^{2-} -capped CdSe QDs of four different sizes. The TEM images of the four QDs are labeled according to the size obtained from steady-state absorption spectra.¹ The panels (i)–(l) show the size distributions and average QD sizes of the TOPO-capped QDs obtained from TEM image analysis using imageJ 1.53a program.²

Table S1 QD sizes determined from steady-state absorption spectra¹, and TEM image analysis, and the three lowest energy transitions observed in the steady-state absorption spectra for the TOPO-capped QDs.

| QD size/ diameter | | 1S | | 2S | | 1P | |
|-------------------|---------|-----|------|-----|------|-----|------|
| nm | | nm | eV | nm | eV | nm | eV |
| Abs. spectra | TEM | | | | | | |
| 2.6 | 3.0±0.5 | 528 | 2.35 | 496 | 2.50 | 426 | 2.91 |
| 3.4 | 3.8±0.7 | 564 | 2.20 | 537 | 2.31 | 458 | 2.71 |
| 4.0 | 4.2±0.4 | 585 | 2.12 | 555 | 2.23 | 504 | 2.46 |
| 4.8 | 4.9±0.7 | 606 | 2.05 | 581 | 2.13 | 529 | 2.34 |

FT-IR spectroscopy

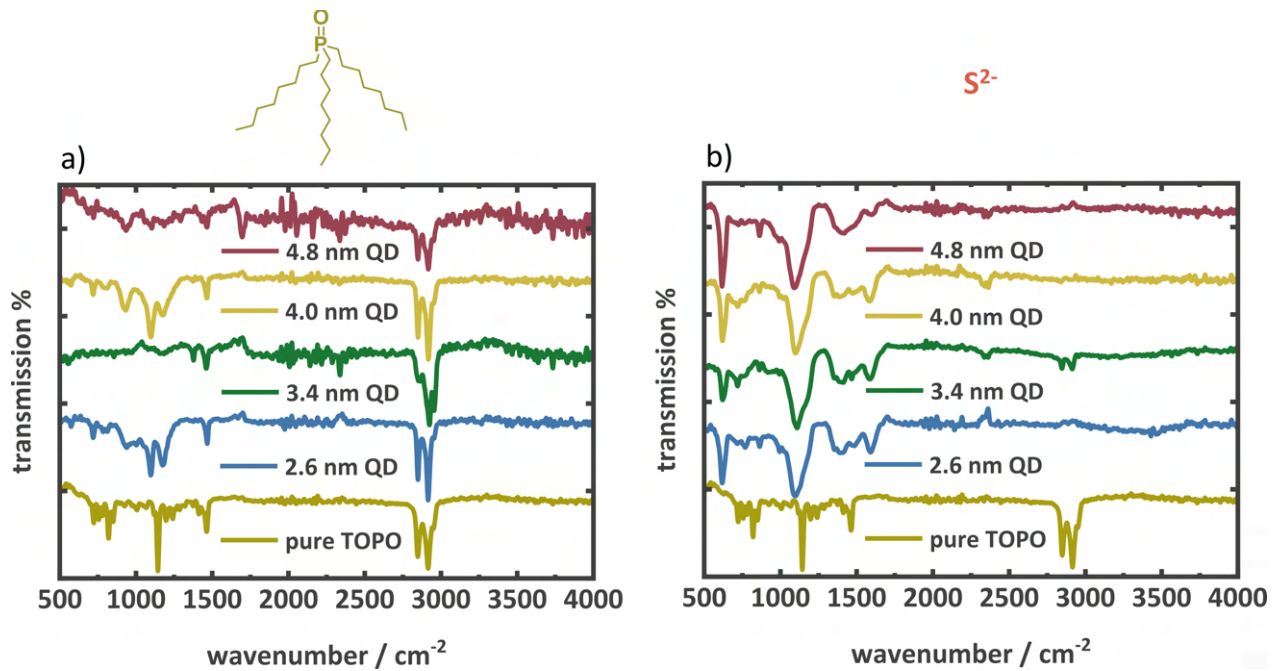


Fig. S2: FT-IR spectra of the (a) TOPO-capped, and (b) S²⁻-capped QDs of four different sizes. A spectrum of the pure TOPO is plotted together with the QD spectra. In Panel (b), it is clear that the TOPO vibration bands are absent in the S²⁻-capped QDs. However, contribution of residual NMF is observed in the S²⁻-capped QDs.

Photoluminescence spectroscopy

To do a quantitative evaluation, the photoluminescence spectra were deconvoluted using two gaussian functions considering the band edge and the trap emission part as shown in Fig. S3a. The extent of band-edge photoluminescence quenching and the enhancement of trap state emission upon S^{2-} functionalization is described by the relative areas obtained from the two fitted gaussians (Fig. S3).

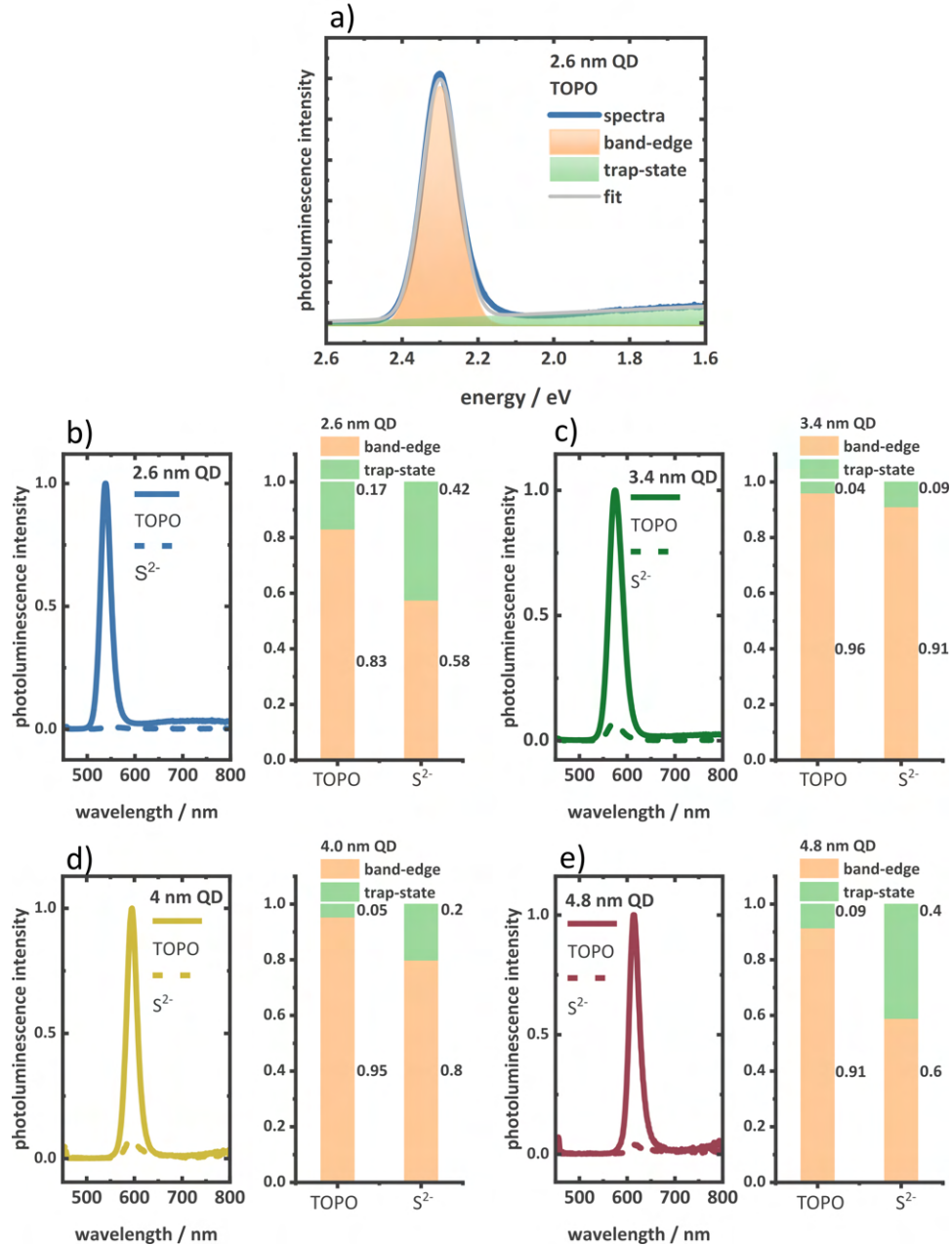


Fig. S3: (a) Gaussian fitting of photoluminescence spectra to evaluate the contribution of band-edge and trap-state contribution. Photoluminescence spectra (λ_{ex} 400 nm) of (b) 2.6 nm, (c) 3.4 nm, (d) 4.0 nm and (e) 4.8 nm, TOPO-capped and S^{2-} -capped QDs. The right panels in the figures demonstrate the relative band-edge and the trap-state emission contribution obtained from the areas of the two gaussians as demonstrated in (a).

Transient absorption spectroscopy

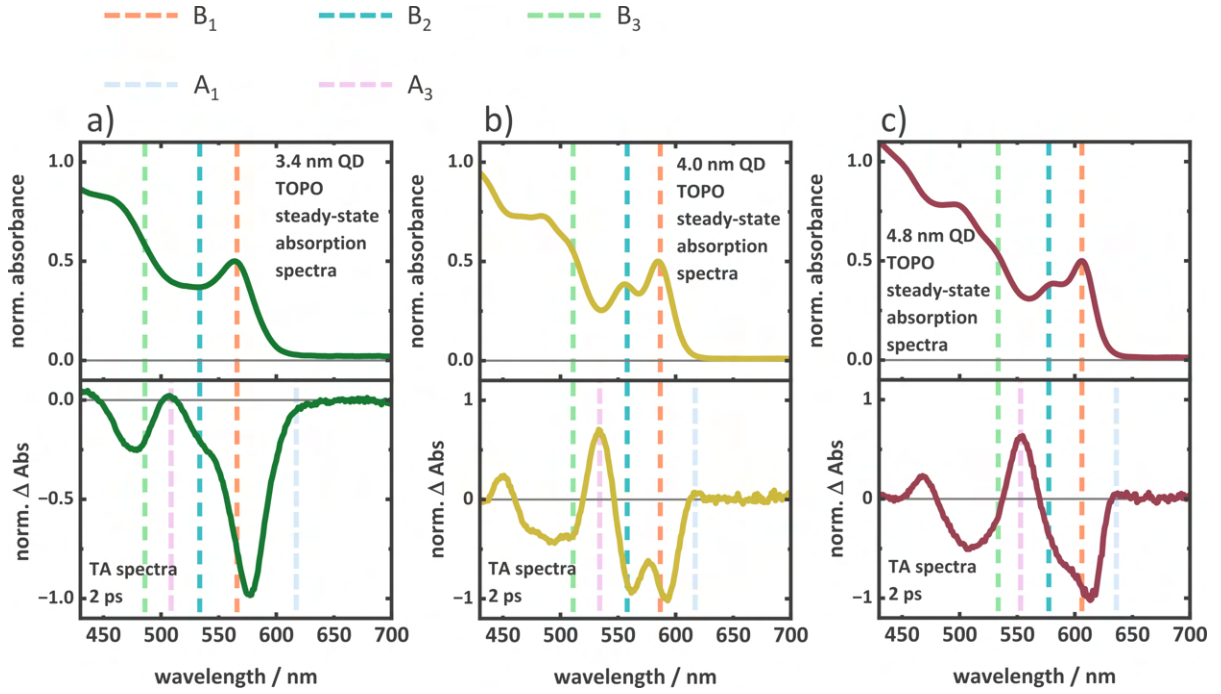


Fig. S4: Comparison of steady-state spectra and TA spectra (1900 ps) of the TOPO-capped QDs of 3.4 nm, 4.0 nm, and 4.8 nm.

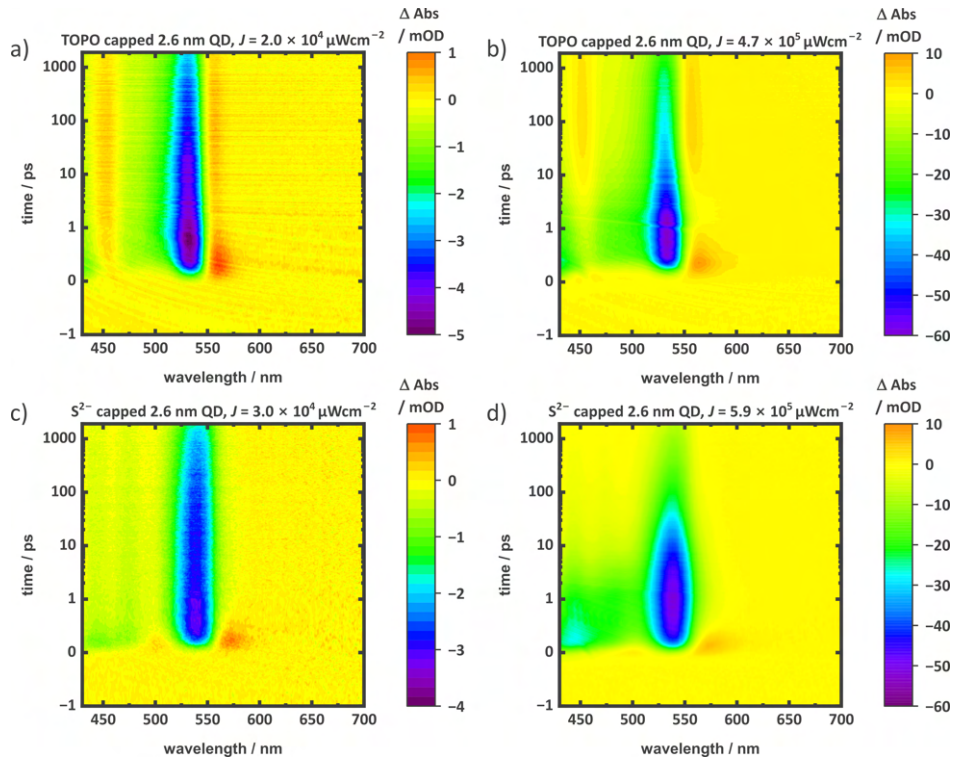


Fig. S5: TA colour map of TOPO-capped 2.6 nm QD at (a) lowest intensity of $2.0 \times 10^4 \mu\text{Wcm}^{-2}$ and, (b) highest intensity $4.7 \times 10^5 \mu\text{Wcm}^{-2}$. TA colour map of S^{2-} -capped 2.6 nm QD at (c) lowest intensity of $2.0 \times 10^4 \mu\text{Wcm}^{-2}$ and, (d) highest intensity $4.7 \times 10^5 \mu\text{Wcm}^{-2}$.

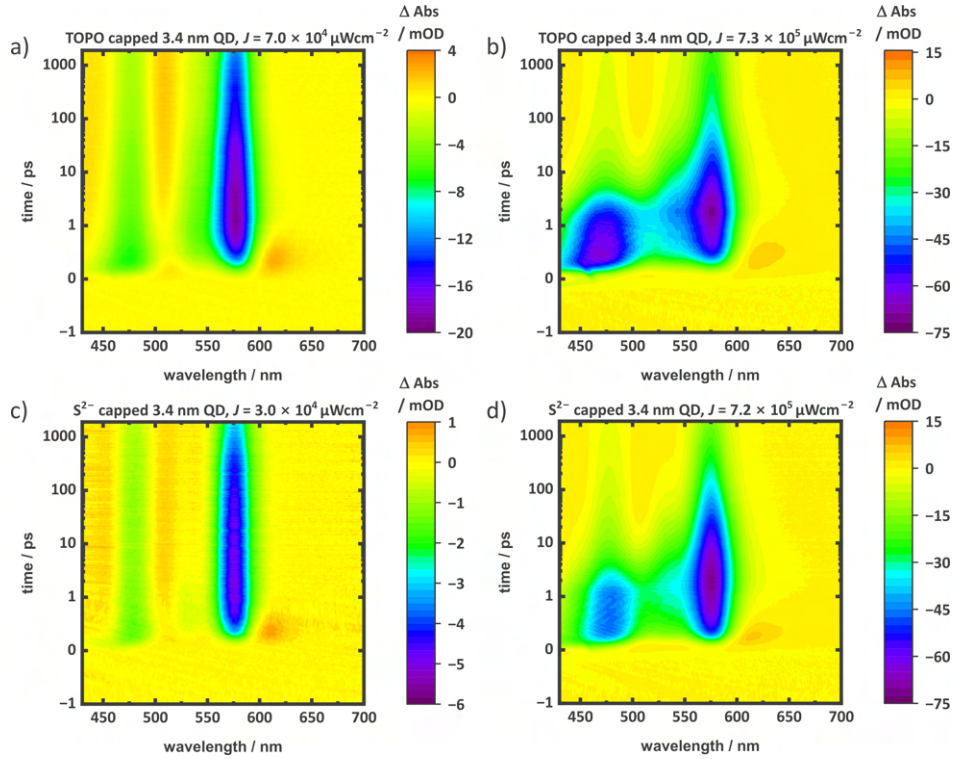


Fig. S6: TA colour of map of TOPO-capped 3.4 nm QD at (a) lowest intensity of $7.0 \times 10^4 \mu\text{Wcm}^{-2}$ and, (b) highest intensity $7.3 \times 10^5 \mu\text{Wcm}^{-2}$. TA colour of map of S^{2-} -capped 3.4 nm QD at (c) lowest intensity of $3.0 \times 10^4 \mu\text{Wcm}^{-2}$ and, (d) highest intensity $7.2 \times 10^5 \mu\text{Wcm}^{-2}$.

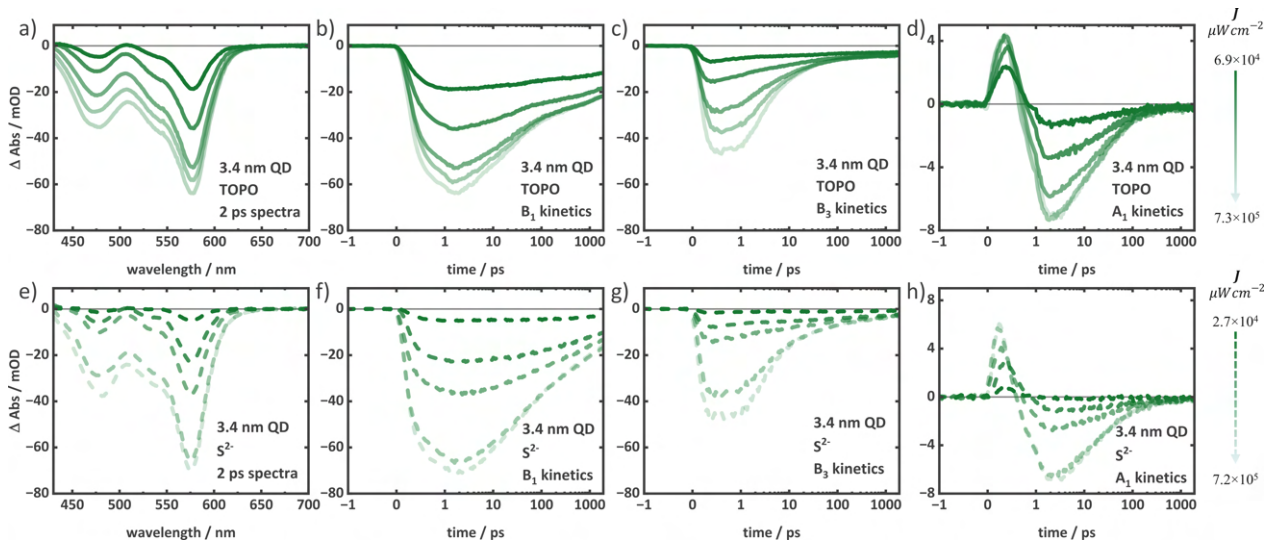


Fig. S7: The intensity-dependent TA data of TOPO-capped 3.4 nm QD depicting (a) spectra at 2 ps, (b) B_1 kinetics, (c) B_3 kinetics, and (d) A_1 kinetics. The intensity-dependent TA data of S^{2-} -capped 3.4 nm QD depicting (e) spectra at 2 ps, (f) B_1 kinetics, (g) B_3 kinetics, and (h) A_1 kinetics. Increasing intensity is represented by the arrows on the right side.

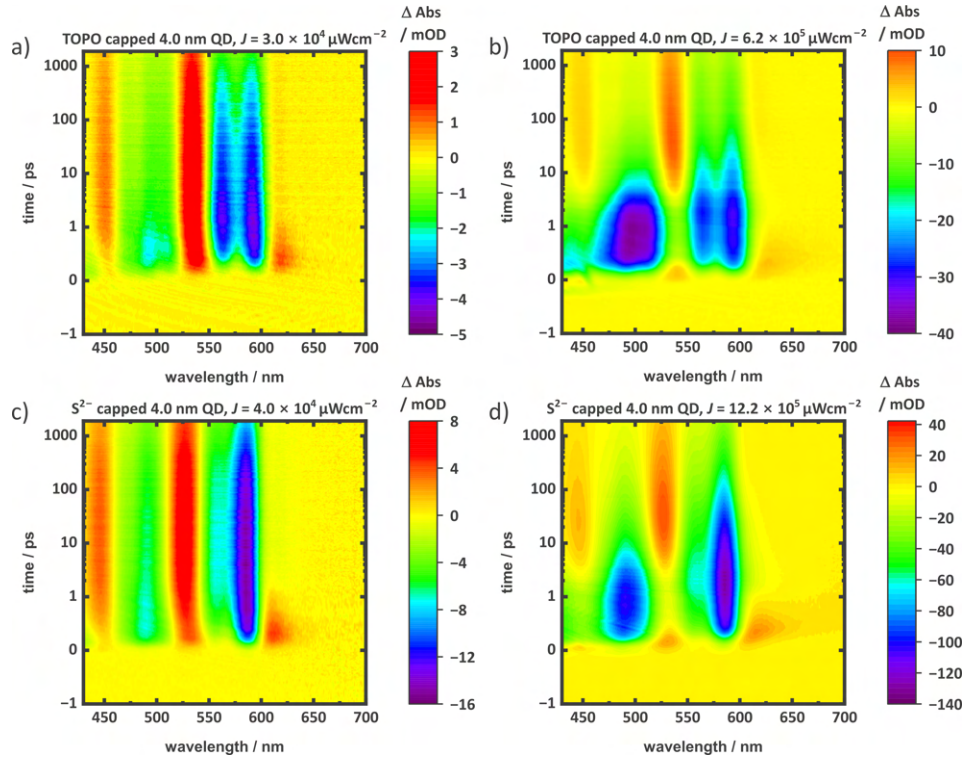


Fig. S8: TA colour of map of TOPO-capped 4.0 nm QD at (a) lowest intensity of $3.0 \times 10^4 \mu\text{Wcm}^{-2}$ and, (b) highest intensity $6.2 \times 10^5 \mu\text{Wcm}^{-2}$. TA colour of map of S^{2-} -capped 4.0 nm QD at (c) lowest intensity of $4.0 \times 10^4 \mu\text{Wcm}^{-2}$ and, (d) highest intensity $12.2 \times 10^5 \mu\text{Wcm}^{-2}$.

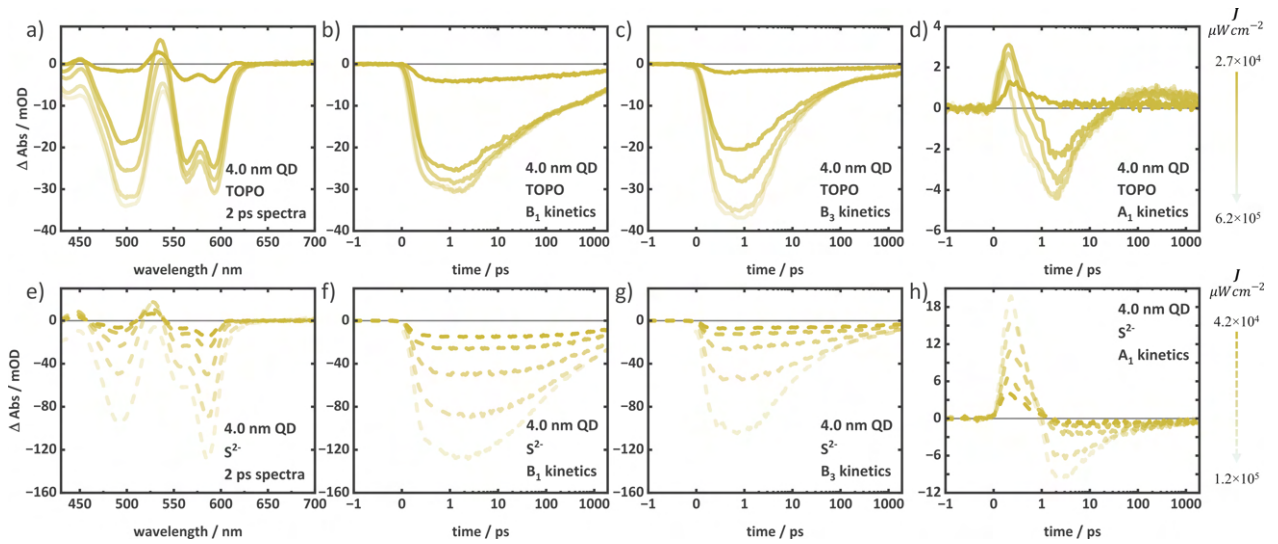


Fig. S9: The intensity-dependent TA data of TOPO-capped 4.0 nm QD depicting (a) spectra at 2 ps, (b) B_1 kinetics, (c) B_3 kinetics, and (d) A_1 kinetics. The intensity-dependent TA data of S^{2-} -capped 4.0 nm QD depicting (e) spectra at 2 ps, (f) B_1 kinetics, (g) B_3 kinetics, and (h) A_1 kinetics. Increasing intensity is represented by the lines on the right side.

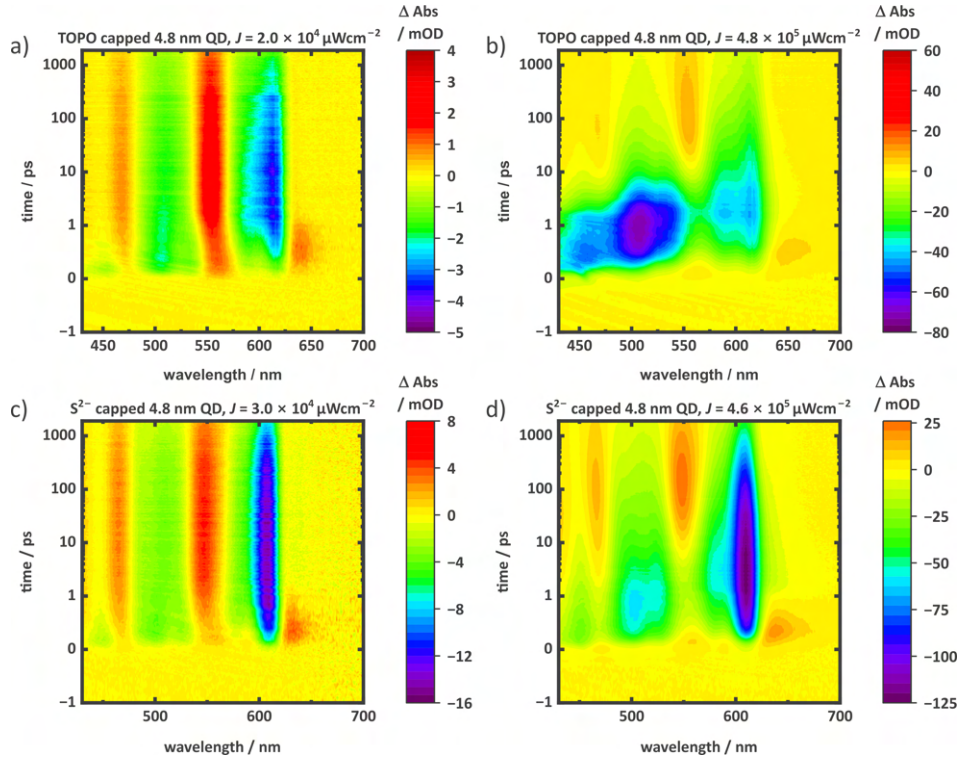


Fig. S10: TA colour of map of TOPO-capped 4.8 nm QD at (a) lowest intensity of $1.0 \times 10^4 \mu\text{Wcm}^{-2}$ and, (b) highest intensity $4.8 \times 10^5 \mu\text{Wcm}^{-2}$. TA colour of map of S^{2-} -capped 4.8 nm QD at (c) lowest intensity of $3.0 \times 10^4 \mu\text{Wcm}^{-2}$ and, (d) highest intensity $4.6 \times 10^5 \mu\text{Wcm}^{-2}$.

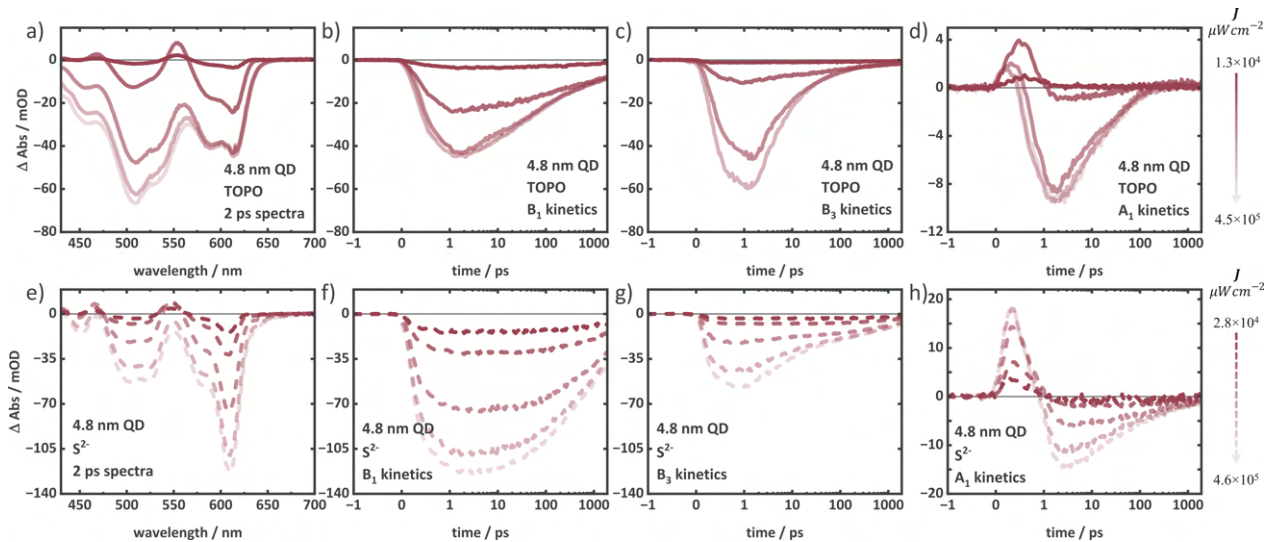


Fig. S11: The intensity-dependent TA data of TOPO-capped 4.8 nm QD depicting (a) spectra at 2 ps, (b) B_1 kinetics, (c) B_3 kinetics, and (d) A_1 kinetics. The intensity-dependent TA data of S^{2-} -capped 4.8 nm QD depicting (e) spectra at 2 ps, (f) B_1 kinetics, (g) B_3 kinetics, and (h) A_1 kinetics. Increasing intensity is represented by the lines on the right side.

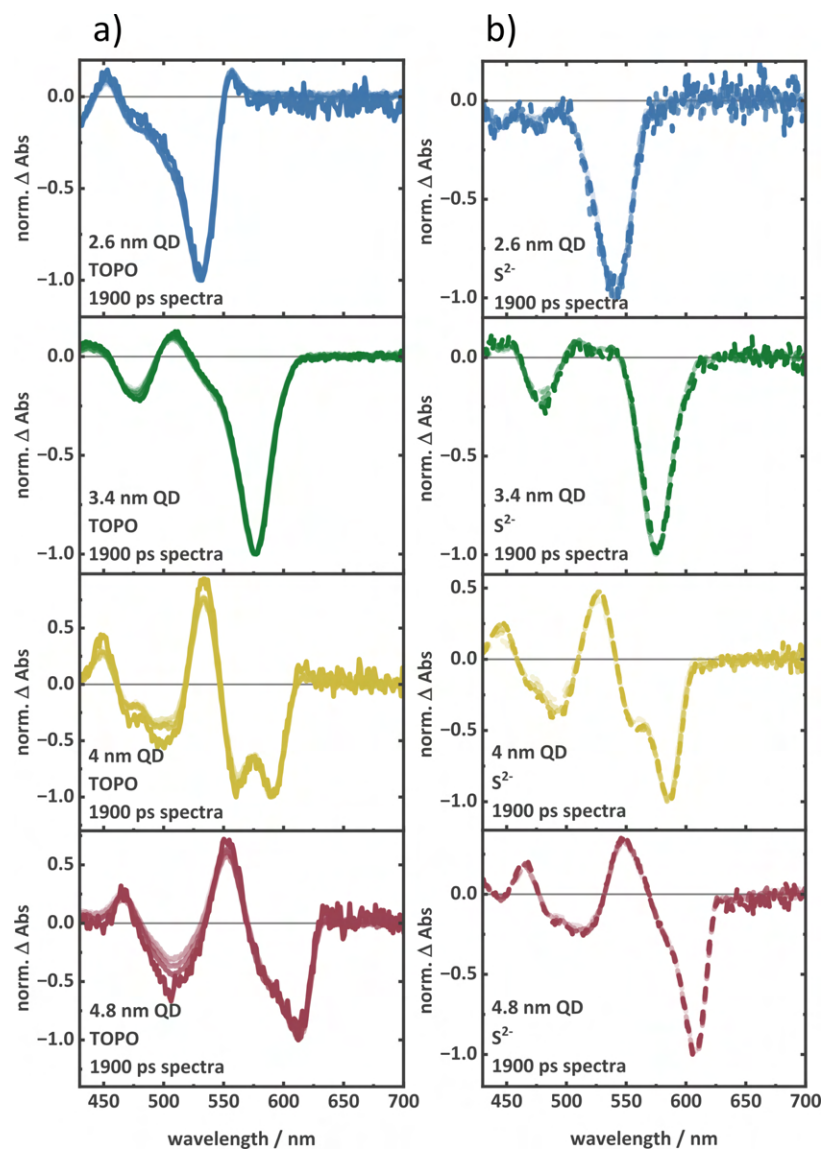


Fig. S12: Intensity-dependent TA spectra (normalized at B_1 bleach) of (a) TOPO-capped and, (b) S^{2-} -capped QDs at 1900 ps.

Determination of absorption cross section

To ensure a reliable MCMC fit result, we firstly compare the α , derived from the fit parameter σ with the α , derived from extinction coefficient³. The extinction co-efficient for the CdSe QDs were determined using the empirical formula demonstrated by Yu et al.¹ Using the extinction co-efficient (ϵ) at 400 nm, we determined the absorption cross section (α) according to the following equation demonstrated by Leatherdale et al.³

$$\alpha_{\epsilon} = \frac{2303 \times \epsilon_{400nm}}{N_a} \quad (1)$$

where, N_a is Avogadro's number

Through the MCMC fit, we obtained an intensity parameter, σ , with which we obtained absorption cross section as,

$$\alpha_{MCMC} = \sigma \times \frac{\text{chopper frequency} \times 10^8}{2.01 \times 10^{12}} \quad (2)$$

The chopper frequency is 500 Hz.

Fig. S13 shows that the α , obtained from σ and extinction co-efficient are not only in the same order of magnitude but also are in good agreement with previous literature³ for all the QDs. This indicates reliable results from MCMC fit.

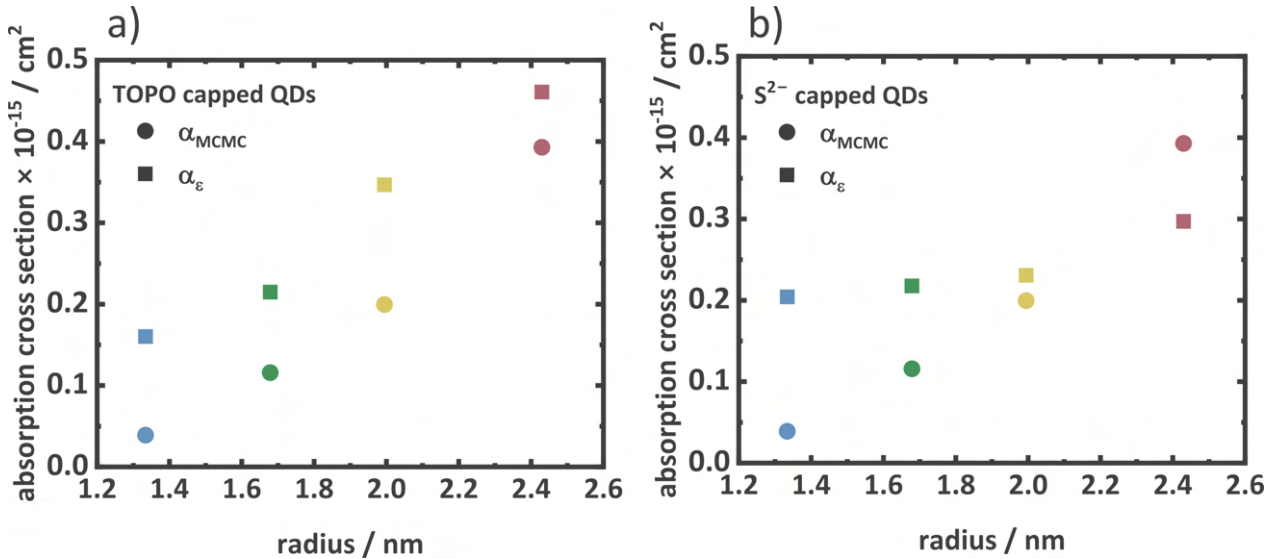


Fig. S13: Absorption cross section obtained from MCMC fit and calculated from the extinction co-efficient. For the TOPO- and S^{2-} -capped QDs.

MCMC fit data

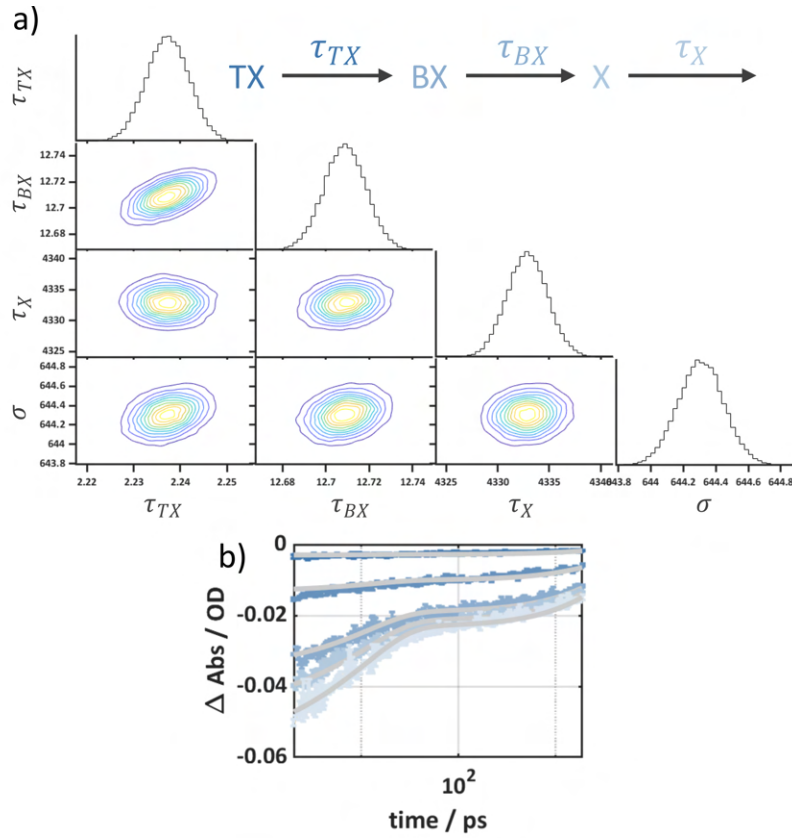


Fig. S14: TX model was used for the MCMC fit of 2.6 nm TOPO-capped QD. (a) Contour plot representing the fit parameters obtained from MCMC. (b) Intensity dependent kinetics of B_1 bleach with the fit (grey lines).

Table S2: Intensities used for the MCMC fit of TOPO-capped 2.6 nm QD and $\langle N \rangle$, σ and, α obtained.

| Intensity $\times 10^8$ μWcm^{-2} | $\langle N \rangle$ | $\sigma \times 10^{-8}$ $\mu\text{W}^{-1}\text{cm}^2$ | α cm^2 |
|---|---------------------|--|---------------------------|
| 0.0002 | 0.1 | 644.1 | 1.6×10^{-15} |
| 0.0008 | 0.5 | | |
| 0.0024 | 1.5 | | |
| 0.0033 | 2.1 | | |
| 0.0047 | 3.0 | | |

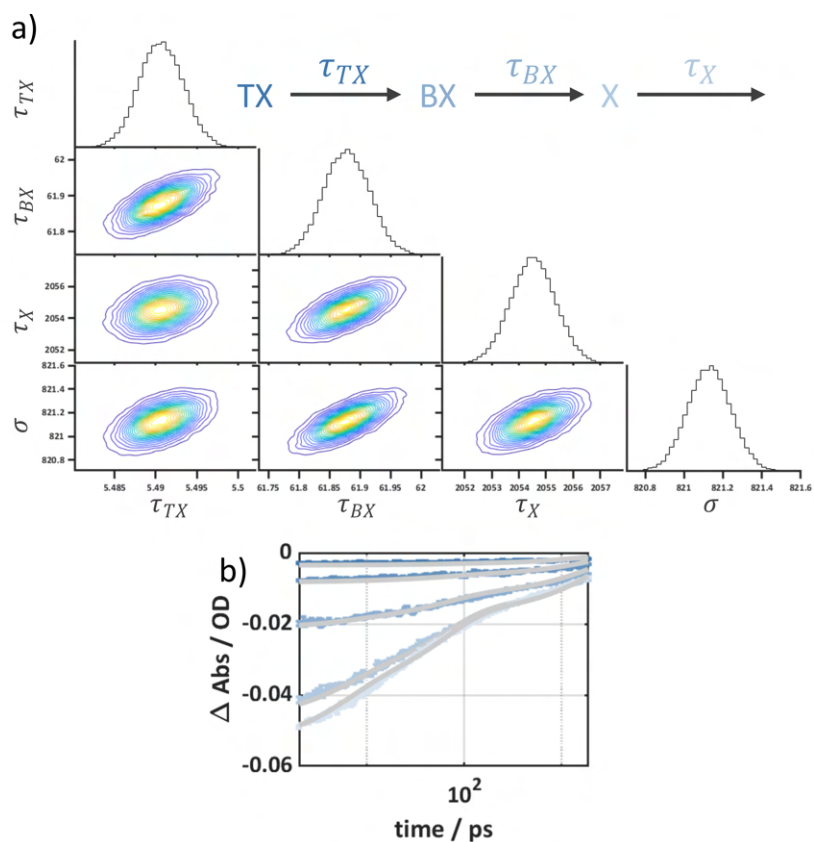


Fig. S15: TX model was used for MCMC fit of 2.6 nm S^{2-} -capped QD. (a) Contour plot representing the fit parameters obtained from MCMC. (b) Intensity dependent kinetics of B_1 bleach with the fit (grey lines).

Table S3: Intensities used for the MCMC fit of S^{2-} -capped 2.6 nm QD and $\langle N \rangle$, σ and, α obtained.

| Intensity $\times 10^8$ μWcm^{-2} | $\langle N \rangle$ | $\sigma \times 10^{-8}$ $\mu\text{W}^{-1}\text{cm}^2$ | α cm^2 |
|---|---------------------|--|---------------------------|
| 0.0003 | 0.2 | 821.1 | 2.0×10^{-15} |
| 0.0006 | 0.5 | | |
| 0.0015 | 1.2 | | |
| 0.0040 | 3.3 | | |
| 0.0059 | 4.8 | | |

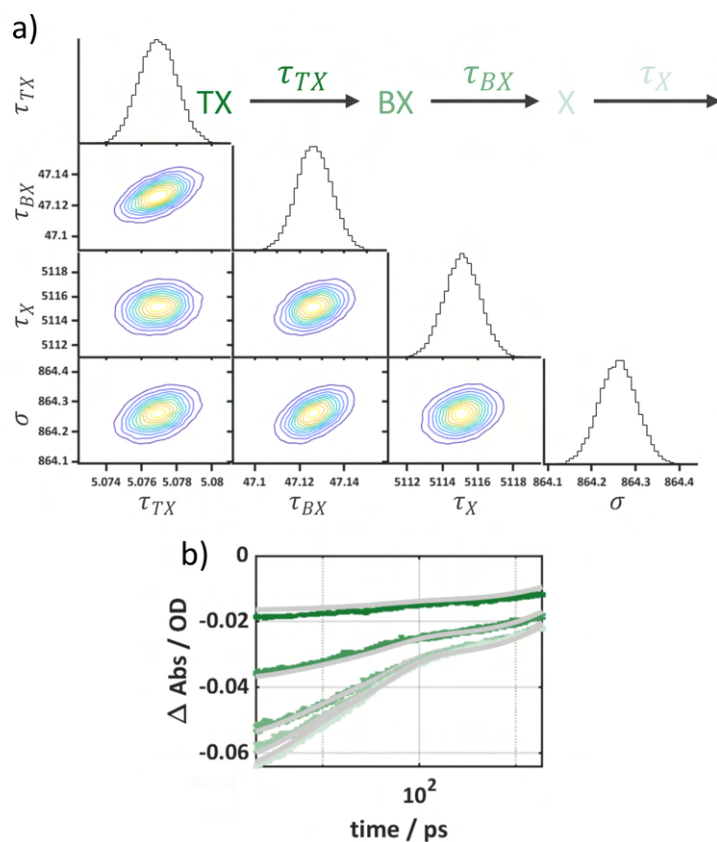


Fig. S16: TX model was used for MCMC fit of 3.4 nm TOPO-capped QD. (a) Contour plot representing the fit parameters obtained from MCMC. (b) Intensity dependent kinetics of B₁ bleach with the fit (grey lines).

Table S4: Intensities used for the MCMC fit of TOPO-capped 3.4 nm QD and $\langle N \rangle$, σ and, α obtained.

| Intensity $\times 10^8$ μWcm^{-2} | $\langle N \rangle$ | $\sigma \times 10^{-8}$ $\mu\text{W}^{-1}\text{cm}^2$ | α cm^2 |
|---|---------------------|--|---------------------------|
| 0.0007 | 0.6 | 864.3 | 2.2×10^{-15} |
| 0.0019 | 1.6 | | |
| 0.0037 | 3.1 | | |
| 0.0053 | 4.5 | | |
| 0.0073 | 6.3 | | |

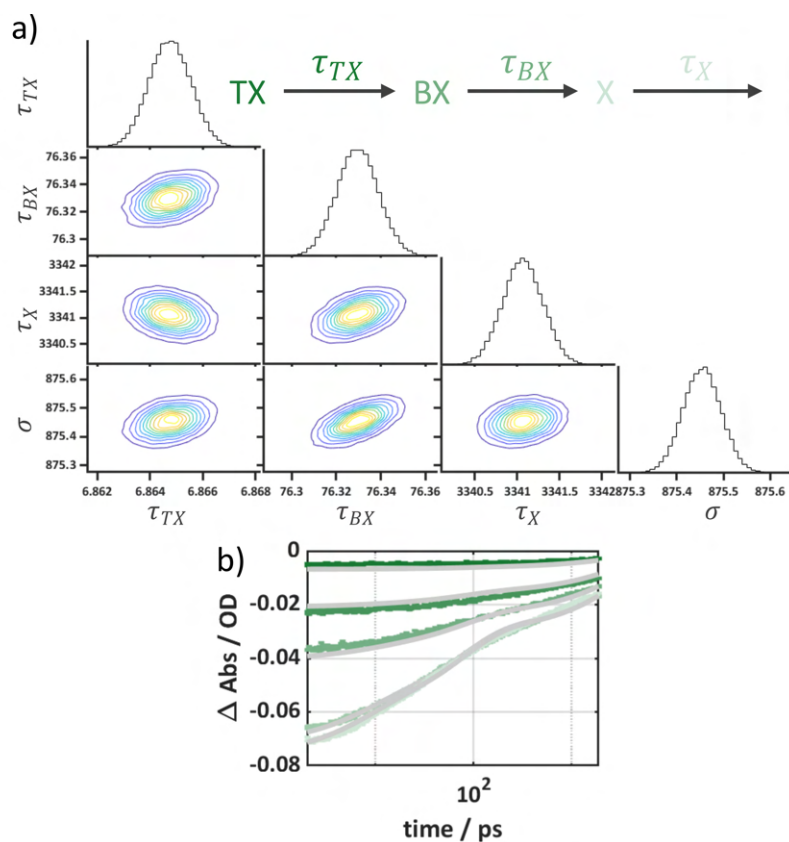


Fig. S17: TX model was used for MCMC fit of 3.4 nm S^{2-} -capped QD. (a) Contour plot representing the fit parameters obtained from MCMC. (b) Intensity dependent kinetics of B_1 bleach with the fit (grey lines).

Table S5: Intensities used for the MCMC fitting of S^{2-} -capped 3.4 nm QD and $\langle N \rangle$, σ and, α obtained.

| Intensity $\times 10^8$ μWcm^{-2} | $\langle N \rangle$ | $\sigma \times 10^{-8}$ $\mu\text{W}^{-1}\text{cm}^2$ | α cm^2 |
|---|---------------------|--|---------------------------|
| 0.0003 | 0.2 | 875.5 | 2.2×10^{-15} |
| 0.0009 | 0.7 | | |
| 0.0018 | 1.6 | | |
| 0.0050 | 4.4 | | |
| 0.0072 | 6.3 | | |

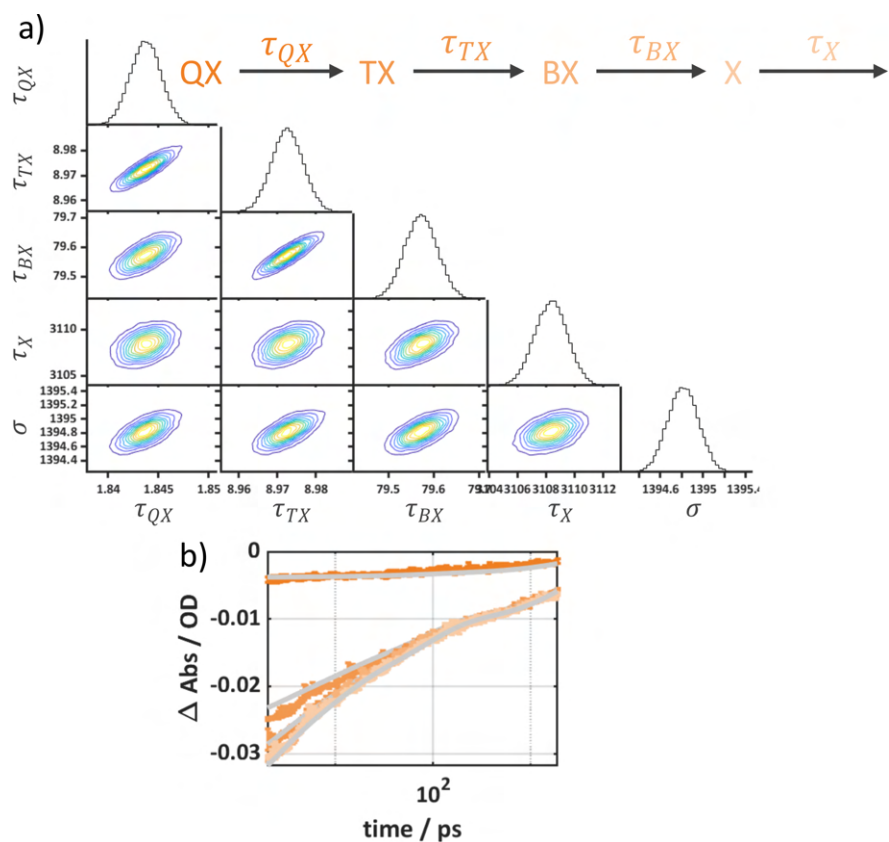


Fig. S18: QX model was used for MCMC fit of 4.0 nm TOPO-capped QD. (a) Contour plot representing the fit parameters obtained from MCMC. (b) Intensity dependent kinetics of B₁ bleach with the fit (grey lines).

Table S6: Intensities used for the MCMC fit of TOPO-capped 4.0 nm QD and $\langle N \rangle$, σ and, α obtained.

| Intensity $\times 10^8$ μWcm^{-2} | $\langle N \rangle$ | $\sigma \times 10^{-8}$ $\mu\text{W}^{-1}\text{cm}^2$ | α cm^2 |
|---|---------------------|--|---------------------------|
| 0.0003 | 0.4 | 1394.8 | 3.5×10^{-15} |
| 0.0022 | 3.0 | | |
| 0.0034 | 4.7 | | |
| 0.0054 | 7.5 | | |
| 0.0062 | 8.6 | | |

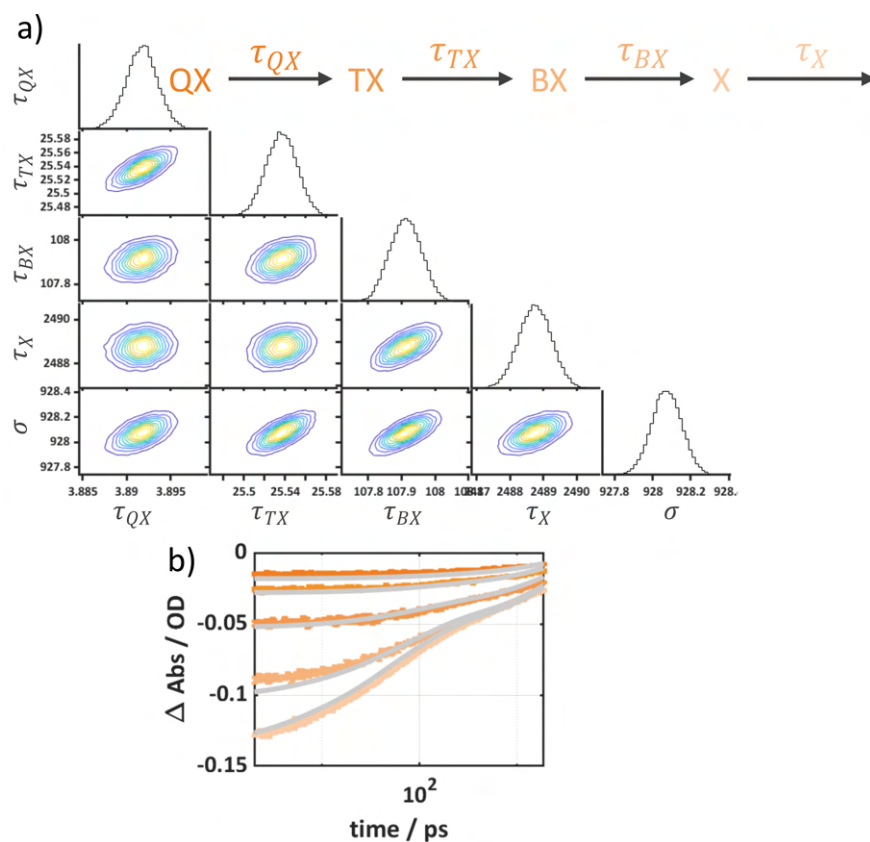


Fig. S19: QX model was used for MCMC fit of 4.0 nm S^{2-} -capped QD. (a) Contour plot representing the fit parameters obtained from MCMC. (b) Intensity dependent kinetics of B_1 bleach with the fit (grey lines).

Table S7: Intensities used for the MCMC fitting of S^{2-} -capped 4.0 nm QD and $\langle N \rangle$, σ and, α obtained.

| Intensity $\times 10^8$ μWcm^{-2} | $\langle N \rangle$ | $\sigma \times 10^{-8}$ $\mu\text{W}^{-1}\text{cm}^2$ | α cm^2 |
|---|---------------------|--|---------------------------|
| 0.0004 | 0.4 | 928.1 | 2.3×10^{-15} |
| 0.0007 | 0.6 | | |
| 0.0014 | 1.3 | | |
| 0.0034 | 3.2 | | |
| 0.0122 | 11.3 | | |

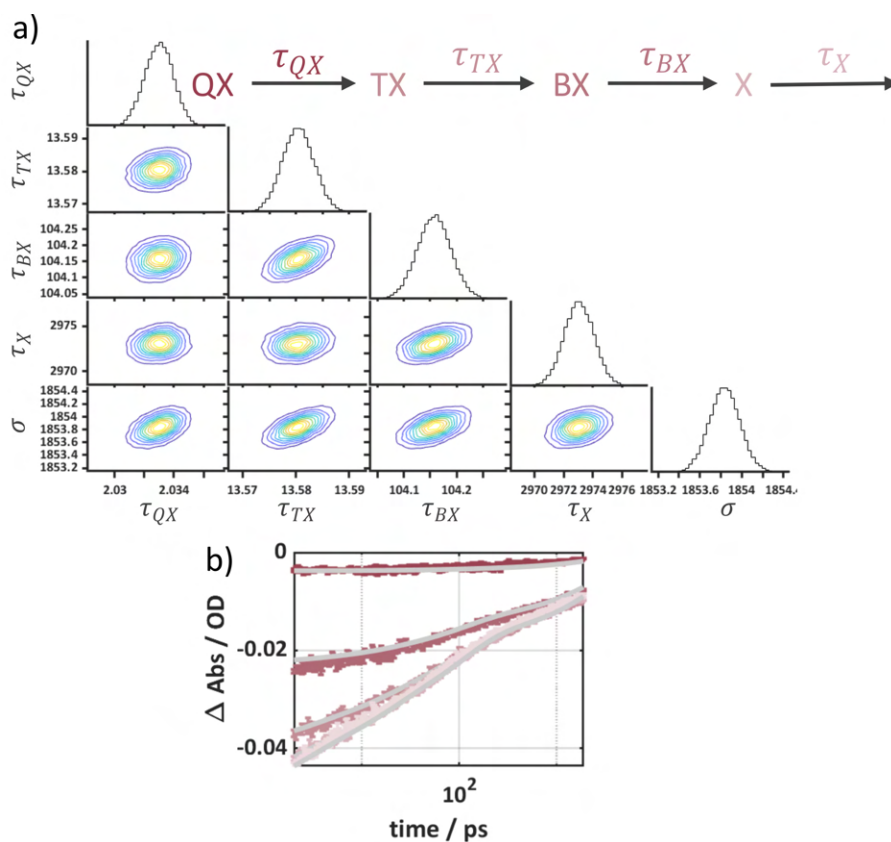


Fig. S20: QX model was used for MCMC fit of 4.8 nm TOPO-capped QD. (a) Contour plot representing the fit parameters obtained from MCMC. (b) Intensity dependent kinetics of B_1 bleach with the fit (grey lines).

Table S8: Intensities used for the MCMC fit of TOPO-capped 4.8 nm QD and $\langle N \rangle$, σ and, α obtained from MCMC fitting.

| Intensity $\times 10^8$ μWcm^{-2} | $\langle N \rangle$ | $\sigma \times 10^{-8}$ $\mu\text{W}^{-1}\text{cm}^2$ | α cm^2 |
|---|---------------------|--|---------------------------|
| 0.0001 | 0.2 | 1853.7 | 4.6×10^{-15} |
| 0.0009 | 1.6 | | |
| 0.0019 | 3.6 | | |
| 0.0030 | 5.6 | | |
| 0.0048 | 8.8 | | |

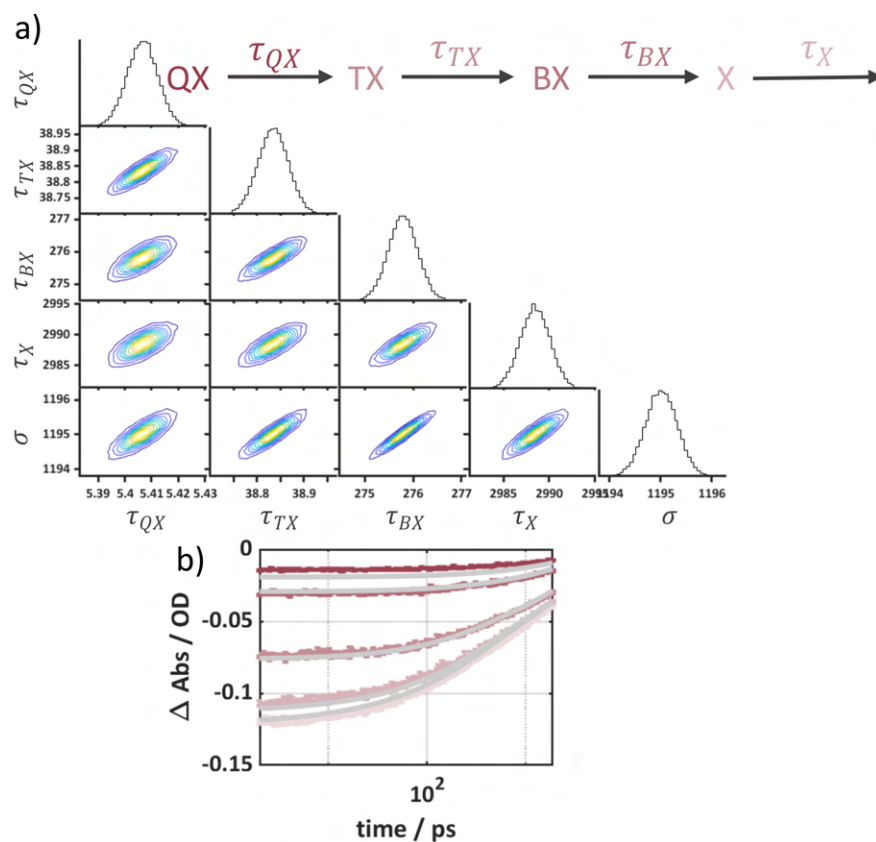


Fig. S21: QX model was used for MCMC fitting of 4.8 nm S^{2-} -capped QD. (a) Contour plot representing the fit parameters obtained from MCMC. (b) Intensity dependent kinetics of B_1 bleach with the fit (grey lines).

Table S9: Intensities used for the MCMC fit of S^{2-} -capped 4.8 nm QD and $\langle N \rangle$, σ and, α obtained.

| Intensity $\times 10^8$ μWcm^{-2} | $\langle N \rangle$ | $\sigma \times 10^{-8}$ $\mu\text{W}^{-1}\text{cm}^2$ | α cm^2 |
|---|---------------------|--|---------------------------|
| 0.0003 | 0.3 | 1195.1 | 2.9×10^{-15} |
| 0.0004 | 0.5 | | |
| 0.0014 | 1.7 | | |
| 0.0033 | 3.8 | | |
| 0.0046 | 5.5 | | |

Multi gaussian fit method to determine multiexciton binding energies

We adapt the multi gaussian fit method described by Labrador et al.⁴ The equations used to model our species spectra are as follows:

$$\begin{aligned}
 S_X(E) = & - \left[A_{B1} \left(e^{-\left(\frac{E-c_{B1}}{w_{B1}}\right)^2} \right) + A_{B2} \left(e^{-\left(\frac{E-c_{B2}}{w_{B2}}\right)^2} \right) \right. \\
 & \left. + A_{B3} \left(e^{-\left(\frac{E-c_{B3}}{w_{B3}}\right)^2} \right) \right]_{GSB} \\
 & + \left[\frac{1}{2} A_{B1} \left(e^{-\left(\frac{E-c_{B1}-\Delta_{BX}}{w_{B1}}\right)^2} \right) + \frac{1}{2} A_{B2} \left(e^{-\left(\frac{E-c_{B2}-\Delta_{BX}}{w_{B2}}\right)^2} \right) \right. \\
 & \left. + A_{B3}^* \left(e^{-\left(\frac{E-c_{B3}^*}{w_{B3}}\right)^2} \right) \right]_{PIA}
 \end{aligned} \tag{3}$$

$$\begin{aligned}
 S_{BX}(E) = & - \left[A_{B1} \left(e^{-\left(\frac{E-c_{B1}}{w_{B1}}\right)^2} \right) + A_{B2} \left(e^{-\left(\frac{E-c_{B2}}{w_{B2}}\right)^2} \right) + A_{B3} \left(e^{-\left(\frac{E-c_{B3}}{w_{B3}}\right)^2} \right) \right]_{GSB} \\
 & + \left[A_{B3}^* \left(e^{-\left(\frac{E-c_{B3}-\Delta_{TX}}{w_{B3}}\right)^2} \right) \right]_{PIA}
 \end{aligned} \tag{4}$$

$$\begin{aligned}
 S_{TX}(E) = & - \left[A_{B1} \left(e^{-\left(\frac{E-c_{B1}}{w_{B1}}\right)^2} \right) + A_{B2} \left(e^{-\left(\frac{E-c_{B2}}{w_{B2}}\right)^2} \right) \right. \\
 & \left. + A_{B3} \left(e^{-\left(\frac{E-c_{B3}}{w_{B3}}\right)^2} \right) \right]_{GSB} + \left[A_{B3}^* \left(e^{-\left(\frac{E-c_{B3}-\Delta_{QX}}{w_{B3}}\right)^2} \right) \right]_{PIA} \\
 & - \left[A_{SE} \left(e^{-\left(\frac{E-c_{SE}}{w_{SE}}\right)^2} \right) \right]_{SE}
 \end{aligned} \tag{5}$$

$$\begin{aligned}
 S_{QX}(E) = & - \left[A_{B1} \left(e^{-\left(\frac{E-c_{B1}}{w_{B1}}\right)^2} \right) + A_{B2} \left(e^{-\left(\frac{E-c_{B2}}{w_{B2}}\right)^2} \right) \right. \\
 & \left. + A_{B3} \left(e^{-\left(\frac{E-c_{B3}}{w_{B3}}\right)^2} \right) \right]_{GSB} + \left[A_{B3}^* \left(e^{-\left(\frac{E-c_{B3}-\Delta_{PX}}{w_{B3}}\right)^2} \right) \right]_{PIA} \\
 & - \left[A_{SE} \left(e^{-\left(\frac{E-c_{SE}}{w_{SE}}\right)^2} \right) \right]_{SE}
 \end{aligned} \tag{6}$$

The S_X , S_{BX} , S_{TX} , and S_{QX} are the species spectra of X, BX, TX, and QX respectively. A represent the amplitudes, c represent the centers, and w represent the widths of the peaks associated to B_1 , B_2 , and B_3 transitions. The subscript GSB accounts for the B_1 , B_2 , and B_3 peaks and the subscript PIA accounts for A_1 , A_2 , and A_3 peaks in the spectra. The widths of the peaks associated with the same transitions are considered the same (e.g., the width of B_1 and A_1 is w_{B1}). The A_3 in the X spectra is not fitted with the same shift (i.e., Δ_{BX}). This is because the $1P_e$ level with higher polarizability than the $1S_e$ level does not necessarily result

in the same magnitude of carrier-induced Stark effect.^{5, 6} Multiexciton binding energy in CdSe QDs is described as bound, i.e., with negative binding energy. Strandell et al.⁷ reports negative multiexciton binding energy upto QX of CdSe QDs of different sizes. Therefore, the positions of A_1 , A_2 , and A_3 peaks are defined by negative shift from the respective B_1 , B_2 , and B_3 bleach positions, which basically determines the binding energy. Similarly, the pentaexciton binding energy (Δ_{PX}) was also assumed to be from a bound pentaexciton state with negative binding energy. The SE feature in CdSe QD TA spectra is not as distinctive as the GSB and PIA. However, it is typically found in resonance with A_1 and B_1 .^{8, 9} In the previous works, SE is fitted by a single Gaussian identical to the 1S gaussian assuming that SE source is the X state.¹⁰ Here, it is fitted with a completely independent Gaussian peak red-shifted from the B_1 to avoid overemphasis of its origin. The SE components in the X and BX spectra were ignored to avoid overparameterization. This is to be clarified that, we do not claim that X and BX spectra do not contain SE contributions. The multiexciton species spectra with the fit of Eq. S3 – Eq. S6 are shown in Fig. S22–S26.

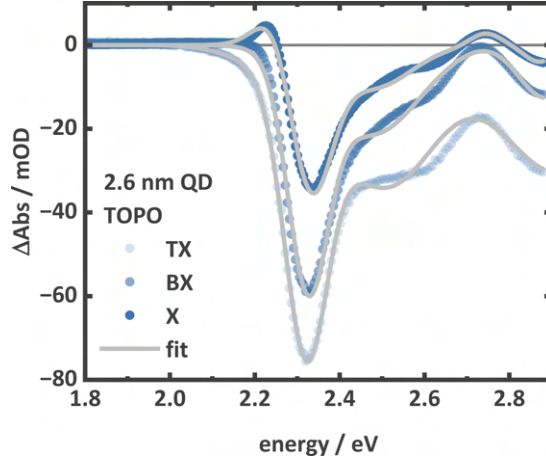


Fig. S22: TX, BX, and X spectra of TOPO-capped 2.6 nm QD along with the respective gaussian fits.

Table S10: Fitting results of gaussian fitting of TX, BX, and X spectra of TOPO-capped 2.6 nm QD.

| | S_X | S_{BX} | S_{TX} |
|-----------------|--|---|---|
| A_{B1} / OD | 0.0513 ^{0.0547} _{0.0479} | 0.0511 ^{0.0539} _{0.0484} | 0.0609 ^{0.0721} _{0.0498} |
| A_{B2} / OD | 0.0182 ^{0.0192} _{0.0172} | 0.0213 ^{0.0220} _{0.0206} | 0.0341 ^{0.0415} _{0.0267} |
| A_{B3} / OD | 0.0040 ^{0.0048} _{0.0032} | 0.0128 ^{0.0266} _{0.0010} | 0.0305 ^{0.0800} _{0.0191} |
| A_{B3}^* / OD | 0.0029 ^{0.0035} _{0.0023} | 0.0010 ^{0.0224} _{-0.0203} | 0.0012 ^{0.0264} _{-0.0026} |
| w_{B1} / eV | 0.0745 ^{0.0767} _{0.0722} | 0.0667 ^{0.0694} _{0.0640} | 0.0715 ^{0.0761} _{0.0670} |
| w_{B2} / eV | 0.1349 ^{0.1512} _{0.1187} | 0.1589 ^{0.1758} _{0.1421} | 0.1800 ^{0.2818} _{0.0782} |
| w_{B3} / eV | 0.0500 ^{0.0683} _{0.0317} | 0.0915 ^{0.2787} _{0.0657} | 0.1835 ^{0.1915} _{0.0824} |
| c_{B1} / eV | 2.3182 ^{2.3195} _{2.3169} | 2.3245 ^{2.3256} _{2.3235} | 2.3197 ^{2.3215} _{2.3180} |
| c_{B2} / eV | 2.4535 ^{2.4687} _{2.4384} | 2.4749 ^{2.4870} _{2.4629} | 2.5069 ^{2.5533} _{2.4606} |
| c_{B3} / eV | 2.8710 ^{2.8844} _{2.8576} | 2.8846 ^{2.9279} _{2.8413} | 2.9100 ^{3.1441} _{2.3242} |
| c_{B3}^* / eV | 2.7434 ^{2.7539} _{2.7330} | | |
| c_{SE} / eV | | | 2.2439 ^{2.3088} _{1.8791} |
| A_{SE} / OD | | | 0.0039 ^{0.0167} _{-0.0090} |
| w_{SE} / eV | | | 0.1341 ^{0.3194} _{0.0513} |
| Δ / eV | 0.0359 ^{0.0378} _{0.0340} | 0.1144 ^{0.1252} _{0.0923} | 0.2036 ^{0.2288} _{0.1916} |

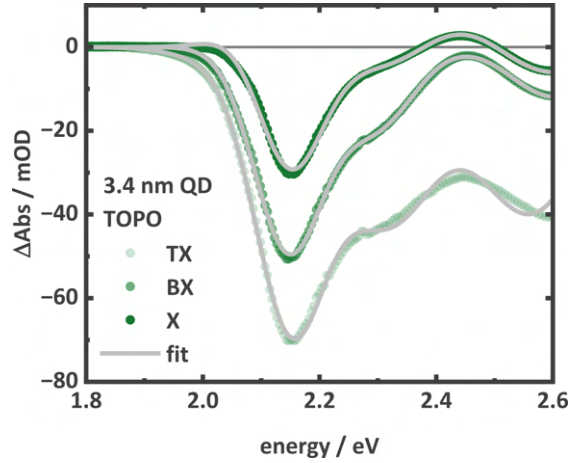


Fig. S23: TX, BX, and X spectra of TOPO-capped 3.4 nm QD along with the respective gaussian fits.

Table S11: Fitting results of gaussian fitting of TX, BX, and X spectra of TOPO-capped 3.4 nm QD.

| | S_X | S_{BX} | S_{TX} |
|-----------------|-----------------------------|-----------------------------|-----------------------------|
| A_{B1} / OD | $0.0507^{0.0585}_{0.0428}$ | $0.0478^{0.0489}_{0.0467}$ | $0.0596^{0.1239}_{0.0047}$ |
| A_{B2} / OD | $0.0157^{0.0613}_{-0.0032}$ | $0.0190^{0.0198}_{0.0182}$ | $0.0415^{0.0734}_{-0.0651}$ |
| A_{B3} / OD | $0.0094^{0.0830}_{-0.0642}$ | $0.0130^{0.2865}_{-0.2604}$ | $0.0397^{0.0622}_{0.0282}$ |
| A_{B3}^* / OD | $0.0110^{0.0948}_{-0.9267}$ | $0.0018^{0.0313}_{-0.3097}$ | $0.0010^{0.0131}_{-0.0129}$ |
| w_{B1} / eV | $0.0820^{0.0864}_{0.0775}$ | $0.0829^{0.0844}_{0.0815}$ | $0.0842^{0.1030}_{0.0653}$ |
| w_{B2} / eV | $0.1225^{0.5380}_{0.0930}$ | $0.0945^{0.1058}_{0.0832}$ | $0.1190^{0.2969}_{0.0258}$ |
| w_{B3} / eV | $0.1324^{0.8045}_{0.0539}$ | $0.1113^{0.6080}_{0.0385}$ | $0.1296^{0.1677}_{0.1083}$ |
| c_{B1} / eV | $2.1363^{2.1410}_{2.1317}$ | $2.1465^{2.1485}_{2.1445}$ | $2.1500^{2.1620}_{2.1280}$ |
| c_{B2} / eV | $2.3174^{2.3910}_{2.2438}$ | $2.2941^{2.2981}_{2.2902}$ | $2.3158^{2.4641}_{2.2674}$ |
| c_{B3} / eV | $2.5600^{2.5817}_{2.4317}$ | $2.5975^{2.6434}_{2.5517}$ | $2.5615^{2.6581}_{2.4650}$ |
| c_{B3}^* / eV | $2.4416^{2.5433}_{2.3601}$ | | |
| c_{SE} / eV | | | $2.0846^{2.1184}_{1.8093}$ |
| A_{SE} / OD | | | $0.0050^{0.0402}_{-0.0302}$ |
| w_{SE} / eV | | | $0.1265^{0.2100}_{0.1057}$ |
| Δ / eV | $0.0242^{0.0269}_{0.0216}$ | $0.0750^{0.0961}_{0.0661}$ | $0.1110^{0.1270}_{0.1023}$ |

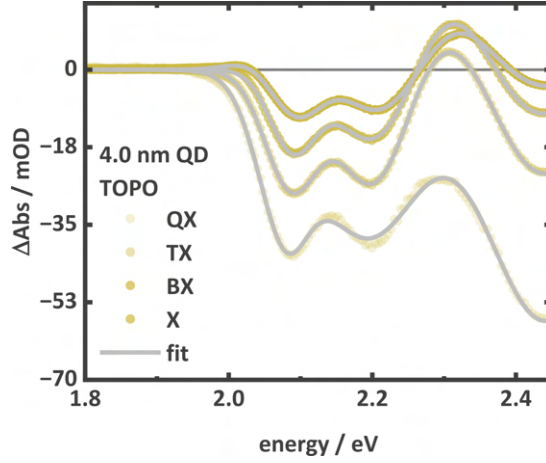


Fig. S24: QX, TX, BX, and X spectra of TOPO-capped 4.0 nm QD along with the respective gaussian fits.

Table S12: Fitting results of gaussian fitting of QX, TX, BX, and X spectra of TOPO-capped 4.0 nm QD.

| | S_X | S_{BX} | S_{TX} | S_{QX} |
|-----------------|--|--|---|---|
| A_{B1} / OD | 0.0180 ^{0.0182} _{0.0178} | 0.0177 ^{0.0182} _{0.0172} | 0.0259 ^{0.0439} _{0.0079} | 0.0247 ^{0.0408} _{0.0087} |
| A_{B2} / OD | 0.0159 ^{0.0163} _{0.0154} | 0.0199 ^{0.0275} _{0.0122} | 0.0289 ^{0.0308} _{0.0270} | 0.0438 ^{0.1374} _{0.0297} |
| A_{B3} / OD | 0.0039 ^{0.0039} _{0.0038} | 0.0205 ^{0.0912} _{0.0087} | 0.0269 ^{0.0468} _{0.0070} | 0.0583 ^{0.1243} _{0.0078} |
| A_{B3}^* / OD | 0.0087 ^{0.0089} _{0.0085} | 0.0241 ^{0.0906} _{0.0185} | 0.0135 ^{0.0349} _{0.0080} | 0.0112 ^{0.2183} _{-0.0190} |
| w_{B1} / eV | 0.0547 ^{0.0555} _{0.0539} | 0.0454 ^{0.0465} _{0.0444} | 0.0516 ^{0.0590} _{0.0441} | 0.0512 ^{0.0601} _{0.0424} |
| w_{B2} / eV | 0.0679 ^{0.0706} _{0.0652} | 0.0748 ^{0.0808} _{0.0688} | 0.0690 ^{0.0729} _{0.0651} | 0.1107 ^{0.1791} _{0.0424} |
| w_{B3} / eV | 0.0624 ^{0.0658} _{0.0590} | 0.0983 ^{0.4693} _{0.0272} | 0.1000 ^{0.1348} _{0.0652} | 0.1200 ^{0.2133} _{0.0267} |
| c_{B1} / eV | 2.0858 ^{2.0864} _{2.0851} | 2.0892 ^{2.0902} _{2.0881} | 2.0873 ^{2.1033} _{2.0712} | 2.0722 ^{2.0820} _{2.0623} |
| c_{B2} / eV | 2.1952 ^{2.1965} _{2.1939} | 2.2100 ^{2.2161} _{2.2038} | 2.2038 ^{2.2061} _{2.2015} | 2.2013 ^{2.4372} _{1.9655} |
| c_{B3} / eV | 2.4401 ^{2.4430} _{2.4372} | 2.3946 ^{2.4291} _{2.2687} | 2.4267 ^{2.4800} _{2.3734} | 2.4377 ^{2.5511} _{2.3243} |
| c_{B3}^* / eV | 2.3193 ^{2.3206} _{2.3181} | | | |
| c_{SE} / eV | | | 2.0415 ^{2.8087} _{1.2744} | 2.0836 ^{2.1007} _{2.0665} |
| A_{SE} / OD | | | 0.0006 ^{0.0180} _{-0.0167} | 0.0046 ^{0.0217} _{0.0012} |
| w_{SE} / eV | | | 0.0535 ^{0.2947} _{0.0187} | 0.0342 ^{0.0677} _{0.0006} |
| Δ / eV | 0.0227 ^{0.0234} _{0.0221} | 0.0662 ^{0.0750} _{0.0550} | 0.1096 ^{0.1277} _{0.0879} | 0.1556 ^{0.2088} _{0.0917} |

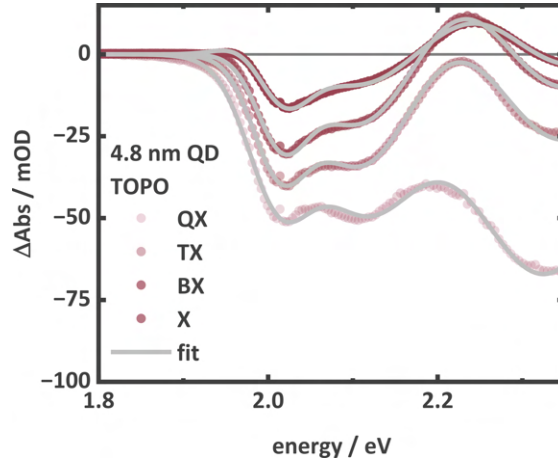


Fig. S25: QX, TX, BX, and X spectra of TOPO-capped 4.8 nm QD along with the respective gaussian fits.

Table S13: Fitting results of gaussian fitting of QX, TX, BX, and X spectra of TOPO-capped 4.8 nm QD.

| | S_X | S_{BX} | S_{TX} | S_{QX} |
|-----------------|--|--|---|---|
| A_{B1} / OD | 0.0237 ^{0.0296} _{0.0177} | 0.0240 ^{0.0268} _{0.0211} | 0.0294 ^{0.0488} _{0.0099} | 0.0353 ^{0.2313} _{0.0160} |
| A_{B2} / OD | 0.0176 ^{0.0231} _{0.0120} | 0.0235 ^{0.0550} _{0.0079} | 0.0368 ^{0.1297} _{-0.0561} | 0.0465 ^{0.0549} _{0.0162} |
| A_{B3} / OD | 0.0052 ^{0.0282} _{0.0017} | 0.0265 ^{0.0888} _{0.0158} | 0.0379 ^{0.0442} _{0.0166} | 0.0675 ^{0.0866} _{0.0162} |
| A_{B3}^* / OD | 0.0111 ^{0.0322} _{0.0100} | 0.0301 ^{0.0835} _{0.0077} | 0.0218 ^{0.0520} _{0.0147} | 0.0011 ^{0.0362} _{0.0009} |
| w_{B1} / eV | 0.0448 ^{0.0477} _{0.0419} | 0.0411 ^{0.0437} _{0.0386} | 0.0442 ^{0.0516} _{0.0369} | 0.0506 ^{0.0859} _{0.0153} |
| w_{B2} / eV | 0.0789 ^{0.1176} _{0.0403} | 0.0836 ^{0.1064} _{0.0608} | 0.0845 ^{0.2004} _{0.0314} | 0.0888 ^{0.2617} _{0.0841} |
| w_{B3} / eV | 0.0781 ^{0.1688} _{0.0126} | 0.0943 ^{0.2024} _{0.0137} | 0.1073 ^{0.1542} _{-0.9397} | 0.1189 ^{0.3535} _{0.0758} |
| c_{B1} / eV | 2.0111 ^{2.0129} _{2.0093} | 2.0158 ^{2.0171} _{2.0145} | 2.0122 ^{2.0143} _{2.0101} | 2.0111 ^{2.0432} _{1.9790} |
| c_{B2} / eV | 2.0958 ^{2.1110} _{2.0806} | 2.1123 ^{2.1679} _{2.0566} | 2.1134 ^{2.1790} _{2.0478} | 2.1130 ^{2.3200} _{2.0961} |
| c_{B3} / eV | 2.2478 ^{2.3402} _{2.1555} | 2.3050 ^{2.6940} _{2.0839} | 2.3227 ^{2.6929} _{2.3074} | 2.3250 ^{2.4271} _{2.3029} |
| c_{B3}^* / eV | 2.3372 ^{2.5614} _{2.1130} | | | |
| c_{SE} / eV | | | 2.0066 ^{2.0790} _{2.0036} | 1.9739 ^{1.9838} _{1.4261} |
| A_{SE} / OD | | | 0.0010 ^{0.0793} _{-0.0773} | 0.0022 ^{0.1441} _{-0.1397} |
| w_{SE} / eV | | | 0.0869 ^{0.9689} _{0.0395} | 0.0615 ^{0.0855} _{0.0324} |
| Δ / eV | 0.0181 ^{0.0199} _{0.0162} | 0.0496 ^{0.0583} _{0.0259} | 0.0708 ^{0.9192} _{0.0477} | 0.1021 ^{0.1278} _{0.0837} |

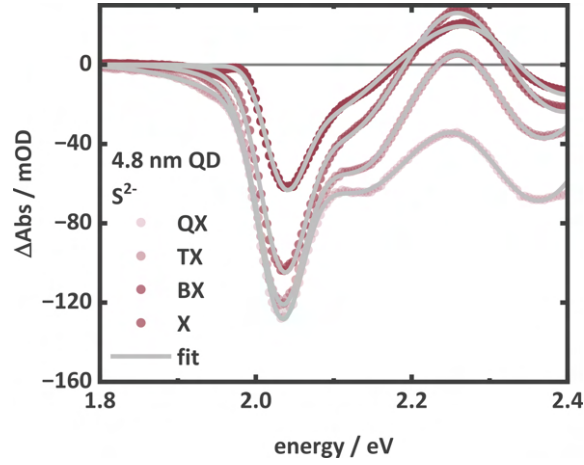


Fig. S26: QX, TX, BX, and X spectra of S^{2-} -capped 4.8 nm QD along with the respective gaussian fits.

Table S14: Fitting results of gaussian fitting of QX, TX, BX, and X spectra of S^{2-} -capped 4.8 nm QD.

| | S_X | S_{BX} | S_{TX} | S_{QX} |
|-----------------|--|---|---|--|
| A_{B1} / OD | 0.0763 ^{0.0905} _{0.0621} | 0.0819 ^{0.0844} _{0.0793} | 0.0971 ^{0.1109} _{0.0833} | 0.0905 ^{0.0980} _{0.0831} |
| A_{B2} / OD | 0.0479 ^{0.0512} _{0.0446} | 0.0394 ^{0.0462} _{0.0326} | 0.0519 ^{0.0721} _{0.0317} | 0.0629 ^{0.1138} _{0.0121} |
| A_{B3} / OD | 0.0275 ^{0.1779} _{-0.1229} | 0.0888 ^{0.0897} _{0.0863} | 0.0521 ^{0.4741} _{-0.3699} | 0.0723 ^{0.0765} _{0.0621} |
| A_{B3}^* / OD | 0.0236 ^{0.1771} _{-0.1299} | 0.0947 ^{0.0953} _{0.0932} | 0.0294 ^{0.4704} _{-0.4116} | 0.0077 ^{0.0079} _{0.0068} |
| w_{B1} / eV | 0.0383 ^{0.0402} _{0.0364} | 0.0401 ^{0.0411} _{0.0390} | 0.0430 ^{0.0449} _{0.0411} | 0.0400 ^{0.0415} _{0.0386} |
| w_{B2} / eV | 0.0850 ^{0.0993} _{0.0707} | 0.0995 ^{0.1067} _{0.0923} | 0.0825 ^{0.1017} _{0.0633} | 0.1149 ^{0.2592} _{0.0295} |
| w_{B3} / eV | 0.0929 ^{0.02007} _{-0.0148} | 0.1048 ^{0.9912} _{-0.7815} | 0.0830 ^{0.1707} _{-0.0048} | 0.0948 ^{0.5287} _{0.0390} |
| c_{B1} / eV | 2.0297 ^{2.0309} _{2.0284} | 2.0348 ^{2.0354} _{2.0343} | 2.0323 ^{2.0328} _{2.0317} | 2.0297 ^{2.0309} _{2.0284} |
| c_{B2} / eV | 2.0721 ^{2.0858} _{2.0583} | 2.1089 ^{2.1234} _{2.0943} | 2.1301 ^{2.1546} _{2.1056} | 2.0721 ^{2.0858} _{2.0583} |
| c_{B3} / eV | 2.3713 ^{2.6776} _{2.0650} | 2.3361 ^{2.3396} _{2.3216} | 2.3501 ^{2.6277} _{2.0725} | 2.3713 ^{2.6776} _{2.0650} |
| c_{B3}^* / eV | 2.2875 ^{2.5563} _{2.0187} | | | |
| c_{SE} / eV | | | 2.0113 ^{2.1830} _{1.8397} | 2.2875 ^{2.5563} _{2.0187} |
| A_{SE} / OD | | | 0.0114 ^{0.0370} _{-0.0142} | 0.0097 ^{0.0600} _{0.0040} |
| w_{SE} / eV | | | 0.0897 ^{0.1636} _{0.0158} | 0.1145 ^{0.2420} _{0.0131} |
| Δ / eV | 0.0129 ^{0.0185} _{0.0074} | 0.0370 ^{0.0394} _{0.0322} | 0.0580 ^{0.0732} _{0.0572} | 0.0646 ^{0.0706} _{0.0514} |

References

- 1 L. Q. W. William Yu, Wenzhuo Guo, and Xiaogang Peng, *Chem. Mater.*, 2003, **15**, 2854-2860.
- 2 C. A. Schneider, W. S. Rasband and K. W. Eliceiri, *Nat Methods*, 2012, **9**, 671-675.
- 3 C. A. Leatherdale, W. K. Woo, F. V. Mikulec and M. G. Bawendi, *J. Phys. Chem. B*, 2002, **106**, 7619-7622.
- 4 T. Labrador and G. Dukovic, *J. Phys. Chem. C*, 2020, **124**, 8439-8447.
- 5 C. Bonati, M. B. Mohamed, D. Tonti, G. Zgrablic, S. Haacke, F. van Mourik and M. Chergui, *Phys. Rev. B*, 2005, **71**.
- 6 Y. Kobayashi and N. Tamai, *J. Phys. Chem. C*, 2010, **114**, 17550-17556.
- 7 D. P. Strandell, A. Ghosh, D. Zenatti, P. Nagpal and P. Kambhampati, *J. Phys. Chem. Lett.*, 2023, **14**, 6904-6911.
- 8 P. Kambhampati, *Acc. Chem. Res*, 2011, **44**, 1-13.
- 9 S. L. Sewall, R. R. Cooney, E. A. Dias, P. Tyagi and P. Kambhampati, *Phys. Rev. B*, 2011, **84**, 235304.
- 10 C. Zhang, T. N. Do, X. W. Ong, Y. T. Chan and H. S. Tan, *Chem. Phys*, 2016, **481**, 157-164.